Univerzita Karlova v Praze
Matematicko-fyzikální fakulta

BAKALÁŘSKÁ PRÁCE

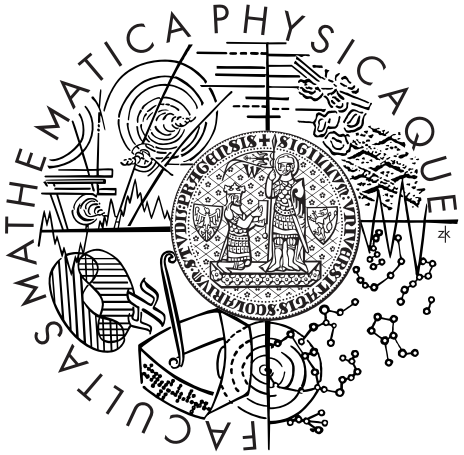

Stanislav Sláčík

Charakterizace strukturních parametrů rozhraní mezi Langmuirovou monovrstvou mastných kyselin a povrchem vody na základě molekulových simulací

Katedra chemické fyziky a optiky

Vedoucí bakalářské práce: RNDr. Martina Roeselová Ph.D.

Studijní program: Fyzika

Studijní obor: Obecná fyzika

Praha 2011

Charles University in Prague
Faculty of Mathematics and Physics

BACHELOR THESIS

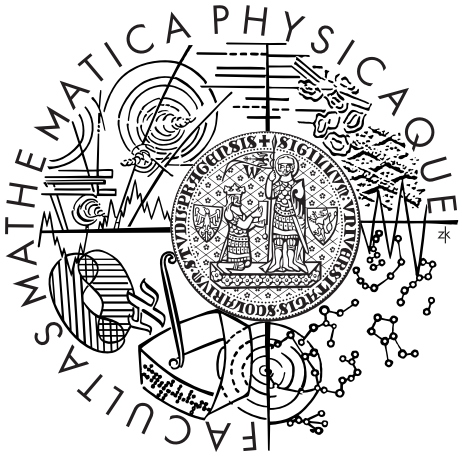

Stanislav Sláčík

Structural characterization of the interface between a fatty acid Langmuir monolayer and water using molecular simulations

Department of Chemical Physics and Optics

Supervisor of the bachelor thesis: RNDr. Martina Roeselová Ph.D.

Study programme: Physics

Specialization: General Physics

Prague 2011

Předložená práce byla z velké části vypracována v Ústavu organické chemie a biochemie Akademie věd ČR, v. v. i.
Chtěl bych touto cestou poděkovat vedoucí bakalářské práce RNDr. Martině Roeselové, PhD. za cenné rady a připomínky k bakalářské práci. Rovněž chci poděkovat Mortezovi Khabirimu, MSc. za pomoc s přípravou simulací.
V neposlední řadě chci poděkovat rodičům za podporu a klidné zázemí během studia.

A large part of the present thesis was done at the Institute of Organic Chemistry and Biochemistry of Academy of Sciences of the Czech Republic.
I would like to aknowledge the helpful advice of the bachelor thesis supervisor RNDr. Martina Roeselová, PhD. The help of Morteza Khabiri, MSc. concerning the preparation of the simulations is appreciated as well.
Moreover I would like to aknowledge my parents, who provided generous support during the studies.

Prohlašuji, že jsem tuto bakalářskou práci vypracoval samostatně a výhradně s použitím citovaných pramenů, literatury a dalších odborných zdrojů.

Beru na vědomí, že se na moji práci vztahují práva a povinnosti vyplývající ze zákona č. 121/2000 Sb., autorského zákona v platném znění, zejména skutečnost, že Univerzita Karlova v Praze má právo na uzavření licenční smlouvy o užití této práce jako školního díla podle §60 odst. 1 autorského zákona.

V ..... dne ..... Podpis autora

I declare that I carried out this bachelor thesis independently, and only with the cited sources, literature and other professional sources.

I understand that my work relates to the rights and obligations under the Act No. 121/2000 Coll., the Copyright Act, as amended, in particular the fact that the Charles University in Prague has the right to conclude a license agreement on the use of this work as a school work pursuant to Section 60 paragraph 1 of the Copyright Act.

In..... date..... signature

Název práce: Charakterizace strukturních parametrů rozhraní mezi Langmuirovou monovrstvou mastných kyselin a povrchem vody na základě molekulových simulací

Autor: Stanislav Sláčík

Katedra: Katedra chemické fyziky a optiky

Vedoucí bakalářské práce: RNDr. Martina Roeselová Ph.D. , ÚOCHB AV ČR, v. v. i.

Abstrakt: V této práci jsou studovány strukturní vlastnosti Langmuirovy monovrstvy palmitové kyseliny ($CH_3(CH_2)_{14}COOH$) na rozhraní voda-vzduch analýzou připravených molekulárně dynamických simulací. Získané veličiny jsou porovnány s dostupnými výsledky z experimentů a souvisejících počítačových simulací publikovaných v literatuře. Byla nalezena shoda s dostupnými údaji v úhlu náklonu alkylových řetězců, hustotních profilech monovrstvy a v tloušťce monovrstvy. Dále bylo zjištěno, že rozdělení délky alkylového řetězce palmitové kyseliny je bimodální; tento jev byl dán do souvislosti s konformací řetězce v oblasti C^1-C^2-C^3-C^4 a pro srovnání byly provedeny simulace hexadekan-1-olu.

Klíčová slova: Langmuirova monovrstva, mastné kyseliny, molekulární dynamika

Title: Structural characterization of the interface between a fatty acid Langmuir monolayer and water using molecular simulations

Author: Stanislav Sláčík

Department: Department of Chemical Physics and Optics

Supervisor: RNDr. Martina Roeselová Ph.D., IOCB CAS

Abstract: The structural properties of a palmitic acid ($CH_3(CH_2)_{14}COOH$) monolayer at the water-air interface are investigated in the present study via analysis of molecular dynamics simulation trajectories. The values are compared to known relevant experimental and computer simulation results, finding good agreement in terms of tilt angle of the chains, monolayer density profiles, and monolayer thickness. The alkyl chain length distribution for palmitic acid was found bimodal and the phenomenon was attributed to the C^1-C^2-C^3-C^4 dihedral angle distribution. Simulations of 1-hexadecanol were carried out for comparison.

Keywords: Langmuir monolayer, fatty acids, molecular dynamics

Contents

Introduction

Surfaces and phase interfaces are studied intensively in various branches of physics, namely condensed matter physics, plasma physics and physical chemistry. Concerning the transport of matter between phases, an important process investigated is the *adsorption* – accumulation of a chemical component at the interface. We are interested especially in the water-air interface for its ubiquity and its meaning for various processes related to life on Earth. Among numerous examples of water-air interfaces are the microscopic aqueous droplets dispersed in the air – the atmospheric *aerosol*, which also contains a large fraction of organic matter of various chemical composition.

The importance of water as a polar solvent led to a distinction between *hydrophilic* and *hydrophobic* behaviour – the tendency to attract or repel water, respectively. Substances manifesting ambiguous behaviour due to presence of both hydrophilic and hydrophobic moieties in their molecules, are called *amphiphilic*. The hydrophobic property restrains the substance from dissolving in water, but the hydrophilic group keeps the molecules in proximity of water, i. e. at the interface. The amphiphiles tend to form *mono*molecular *layers* provided that the molecules have enough space to arrange at the water surface. Such system – a monomolecular layer of insoluble liquid at the air-water interface – is called the *Langmuir monolayer* in the honour of Irving Langmuir, who began to look into monolayer properties systematically in 1910s [1].

It is assumed that organic amphiphiles, foremost carboxylic acids with chains up to 32 carbon atoms long, form a monolayer at the surface of aerosol particles [2]. The presence of the monolayer affects water uptake into the particles as well as the evaporation from them. This impacts consequently various atmospheric processes, for instance cloud formation. For laboratory experiments purpose, Langmuir monolayers of relevant substances are formed in special devices and their properties are measured by e. g. X-ray diffraction and infrared spectroscopy. However, recent rapid progress in computer performace made possible to study these systems also by means of computer simulations.

An objective of the present thesis is to analyse existing data from molecular dynamics simulations of palmitic acid monolayer at the air-water interface, assess their adequacy and run additional simulations when necessary. The ultimate purpose of the analysis is to determine the suitability of the simulation parametres for use in further simulations of atmospherically relevant surfaces.

The first chapter is devoted to theoretical background of the study; general properties of organic monolayers are discussed in the first section, while the second section reveals the basics of the approach used, the molecular dynamics. Second chapter describes the molecular dynamics simulations which served as source of data for analysis and gives an overview of the analysis methodology. The results obtained from the simulations, compared to relevant experimental and computer simulation data from the literature, are discussed in the third chapter. Fourth chapter foreshows some perspectives and sums up the achieved results.

1. Theoretical Background

1.1 Langmuir monolayers and self-assembly

Amphiphiles in the water-air system tend to accumulate at the interface. The hydrophilic *headgroup* is anchored among the water molecules, while the hydrophobic *tailgroup* is repelled from water, pointing away from the water surface. A sketch of the monolayer organisation is given in Figure 1.1. The intermolecular force between nonpolar tailgroups is weaker than the polar interactions. Amphiphiles therefore decrease the surface tension of water; the term *surfactant* is often used, particularly when concerning their use in food processing, detergency or cosmetics.

It appears useful for theoretical and experimental purpose to introduce *surface pressure* π in a surfactant film as the difference between surface tension of the neat water γ_0 and surface tension of water with surfactant $\tilde{\gamma}$ [1].

$$\pi = \gamma_0 - \tilde{\gamma} \tag{1.1}$$

At a given temperature one is able to measure the surface pressure with respect to the surface area per surfactant molecule to obtain the *pressure - area isotherm*. An example of the isotherm for palmitic acid monolayer is plotted in Figure 1.2. When the area per molecule s is high (i. e. surface density of the monolayer is low), the tailgroups interact with each other only negligibly. The Langmuir monolayer in this state is referred to as *2D-gas*. When the film is compressed enough, the molecules "condense" and form *2D-liquid* phase. The phase transition is viewed as the change of the isotherm's slope at 0.25 nm^2. Upon further compression the monolayer can undergo another phase transition to form *liquid crystal* phase characterised by high ordering of the molecules. In our example the phase transition occurs at 0.20 nm^2. Such film collapses when compressed beyond a certain threshold, as it is viewed in sharp decrease of surface pressure at 0.18 nm^2.

A device designed to form and study Langmuir monolayers, equipped with tools to vary the surface density of the monolayer and to measure surface tension, is called *Langmuir trough*. Due to vulnerability of a monolayer to impurities the trough is made of a chemically inertial material. Troughs are often used to deposit

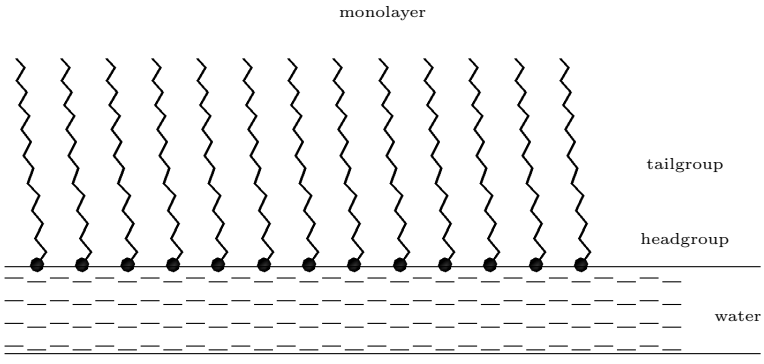

Figure 1.1: Schematic picture of the amphiphilic monolayer organisation.

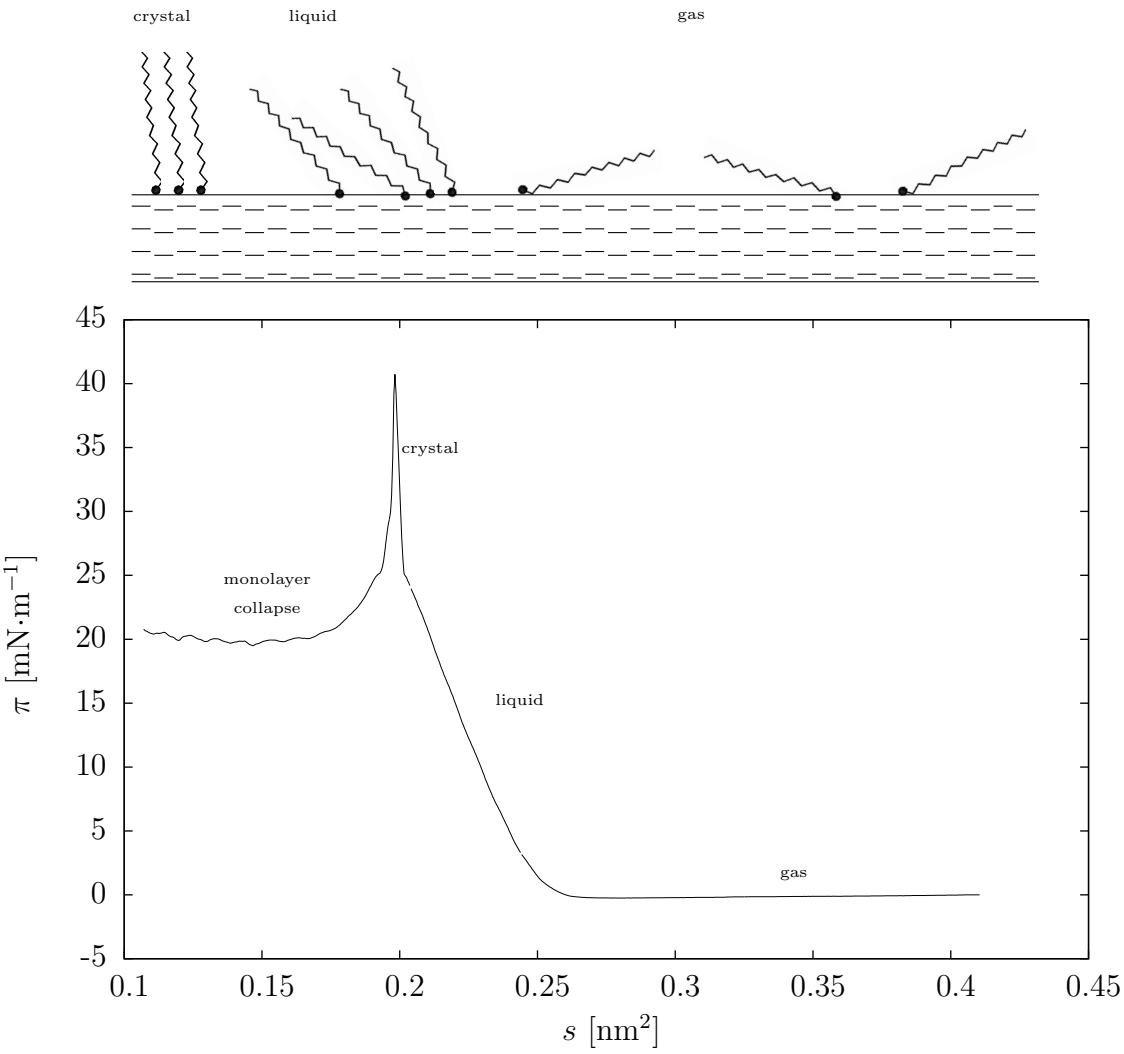

Figure 1.2: Pressure – area isotherm of the palmitic acid monolayer at 22°C. *Data courtesy of Sierra-Hernández and Allen. [2]*

the monolayer from water onto a solid substrate to form the Langmuir-Blodgett film. The process of deposition can be repeated in order to obtain surface layer of desired thickness and is employed in e. g. antireflection, UV-resistance or anti-fog treatment of glass. The resemblance of Langmuir-Blodgett film to cell membrane structures provides ground for research in biochemistry and bionics.

The experimental techniques for studying structural properties of monolayers include infrared reflection absorption spectroscopy (IRRAS) [2] and X-ray grazing incidence diffraction (GID) [3]. Both employ steep angle of the incident wave to overcome the small thickness of the layer. The former enables to obtain the vibrational spectra of the molecules, while the latter provides insight into molecular arrangement of the monolayer – the packing density and orientation of the tailgroups. Sum frequency generation (SFG) is another spectroscopic method, using two beams of different frequencies, one visible and one infrared, which produce a beam of frequency equal to the sum of the original ones. An advantage of SFG is the surface selectivity [2]. Optical microscopy is also employed, often using Brewster angle of the incident light to suppress contributions beyond the

interface [2].

1.2 Molecular dynamics

Various physical processes, especially those involving many-body interaction, are being investigated by a distinct branch of computer simulations - the molecular dynamics (often abbreviated as MD.) Classical MD system is modelled as a system of N interacting particles (e. g. atoms), obeying Newton's equations of motion

$$\mathbf{F}_i = m_i \frac{\mathrm{d}\mathbf{v}_i}{\mathrm{d}t}, \; i = 1 \ldots N, \tag{1.2}$$

where $\mathbf{F}_i$ is the force acting on the i^{th} particle, m_i the mass and $\mathbf{v}_i$ the velocity of i^{th} particle. The interactions between the particles are described by interaction potentials with empirical parametres and the force is determined as the negative gradient of total potential energy

$$\mathbf{F}_i = -\nabla_i V(\mathbf{r}_1, \ldots, \mathbf{r}_N), \tag{1.3}$$

where $\mathbf{r}_1, \ldots, \mathbf{r}_N$ denote the position vectors of the particles and ∇_i is the symbolic vector of partial derivatives with respect to the coordinates of the i^{th} particle.

The set of potentials and appropriate parametres describing interactions is referred to as a *forcefield*. The parametres are chosen so as to fit the measured thermodynamical properties of considered substances [4]. Another way to obtain the desired forcefield parametres is to determine them from *ab initio* calculations, which employ numerical methods to solve Schrödinger's equation for a system of nuclei and electrons.

A rich variety of forcefields exist. They differ in the approach to a molecule description; those which treat each atom as a separate interaction site are called *all-atom*. Some forcefields, however, do not represent nonpolar hydrogen atoms explicitly; this is the case of *united-atom* forcefields. An even cruder approach of *coarse-grained* forcefields is based on representing whole functional groups as separate interaction sites. Examples of commonly used forcefields include OPLS (both in all-atom and united-atom versions), series of AMBER forcefields or the coarse-grained MARTINI. A number of special forcefields for water exist as well, with SPC/E or TIP4P among the most popular.

The molecular structure, namely the list of bonds along with their lengths and angles, is, in MD nomenclature, known as *topology*. The forcefield information is usually included in the topology as well. Bond strechting and valence angle vibrations can be described via harmonic potentials

$$V_{BS} = \frac{1}{2} k^b_{ij} (r - r_0)^2 \tag{1.4}$$

$$V_{VA} = \frac{1}{2} k^a_{ijk} (\theta - \theta_0)^2. \tag{1.5}$$

These vibrations are, however, often neglected and the bonds and/or the bond angles are considered as *constraints* in the equations of motion [5].

A specific part of intramolecular interaction concerns the *dihedral angle*. Defined for four points $ABCD$, the dihedral angle ϕ is the angle between planes

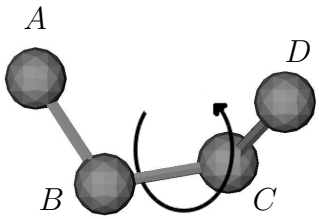

Figure 1.3: The dihedral angle.

ABC and BCD; Figure 1.3 illustrates the definition. Basically, the dihedral angle interaction corresponds to the rotation around the BC axis, thus it is described by a periodic potential, which one can rewrite in Fourier series. Moreover, the function is even, so the series is equivalent to expansion

$$V_{RB} = \sum_n c_n \cos^n \phi, \tag{1.6}$$

which is slightly easier to compute than the Fourier series. For MD applications the expansion in first four or five terms suffices [7]; in this case the potential (1.6) is referred to as Ryckaert–Bellemans potential.

In addition to the above intramolecular (*bonded*) interactions, there are also interactions between atoms not linked to each other via covalent bonds – the *non-bonded* interactions. The dispersion and repulsion term of the van der Waals interaction can be described with the Lennard-Jones potential, often written in the form

$$V_{LJ} = 4\varepsilon_{ij}\left[\left(\frac{\sigma_{ij}}{r}\right)^{12} - \left(\frac{\sigma_{ij}}{r}\right)^{6}\right], \tag{1.7}$$

where parametres ε_{ij} and σ_{ij} depend on the types of the two interacting atoms. The approach of some models such as OPLS is to specify the parametres $\varepsilon_{ii}, \sigma_{ii}$ for pairs of atoms of the same type. To get the appropriate parametre for arbitrary pair of atom types, $\varepsilon_{ii}, \sigma_{ii}$ and $\varepsilon_{jj}, \sigma_{jj}$ are combined via geometric mean

$$\varepsilon_{ij} = \sqrt{\varepsilon_{ii}\varepsilon_{jj}}.$$

$$\sigma_{ij} = \sqrt{\sigma_{ii}\sigma_{jj}}.$$

Alternative corrections to the repulsive term r^{-12} (such as the Buckingham interaction which employs the exponential function instead) also exist and can provide more realistic description of the intermolecular behaviour, though at a higher computational cost.

When charges are present, the electrostatic interaction, described by Coulomb potential, needs to be considered. The Coulomb potential takes in SI units the form

$$V_{ES} = \frac{1}{4\pi\varepsilon}\frac{q_1 q_2}{r}, \tag{1.8}$$

where r is the distance between atoms, q_1, q_2 are the charges, ε is the permitivity of the environment.

Equations (1.2) are typically solved by algorithms which differ from common ordinary differential equation solver methods such as Euler or Runge-Kutta [6] in terms of derivative evaluation and order of the method, as most MD applications do not require particularly high accuracy. The often used *leapfrog algorithm* [5] is formally described by equations

$$\mathbf{v}(t + \frac{\Delta t}{2}) = \mathbf{v}(t - \frac{\Delta t}{2}) + \frac{\Delta t}{2m}\mathbf{F}(t) \tag{1.9}$$

$$\mathbf{r}(t + \Delta t) = \mathbf{r}(t) + \Delta t \mathbf{v}(t + \frac{\Delta t}{2}). \tag{1.10}$$

At a given step, characterised by time t, the integrator evaluates the forces from the derivatives of the total interaction potential (1.3) as a function of the atom positions and sets the velocity at the half-step. Then it "moves" the atoms - computes the positions at the next step. The positions of atoms are stored in a special file (called *trajectory file*) at regular intervals.

To avoid undesired surface effects arising from simulating a finite (and, in comparison to macroscopic systems, extremely small) system, periodic boundary conditions (PBC) are imposed to a certain range of $\mathbb{R}^3$, which we refer to as the *simulation box*. Whenever an atom exits the box, its periodic image enters the box from the opposite face. Thus PBC can be viewed as if the simulation box is surrounded with periodic copies of itself. This approach involves the minimum image convention – only the nearest of the atom periodic images is considered in short-range intermolecular interactions.

Since evaluation of forces demands most of the CPU time, several algorithms are employed to cut on the computational cost. Apart from constraining intermolecular motions, the short-range[1] interactions such as Lennard-Jones are truncated beyond the *cut-off* distance which is at most half the box size due to minimum image convention. For Coulomb interaction, however, the cut-off method is often inaccurate; the particle mesh Ewald (PME) method [8], which takes the advantage of periodic boundary conditions, is then used to reach a desirable accuracy of the electrostatic force. The aim of PME is to decompose the potential into short- and long-range parts, evaluating the convolution in the latter part via discrete Fourier transform [6].

Thermodynamical information is important in exploring macroscopic systems; there are ways to obtain the information from the dynamics of the system by means of statistical mechanics. The simulation needs to be run for sufficient time on the order of (typically) nanoseconds, albeit the time might need to be longer in some situations. By default, the integrator keeps number of atoms N and volume V (due to PBC) constant; total energy E is conserved as a consequence of equations of motion (1.2), hence the *microcanonical ensemble* [9] is sampled. However, since it is often desirable to sample *canonical* (NVT or NpT) ensemble to mimic experimental conditions, external influence on the system needs to be considered. Methods of controlling thermodynamic properties of the system such as the temperature or pressure are known as *coupling*. One of the methods used to maintain desired temperature is to rescale velocities [10] of all atoms so as to

[1] Forces, which are $o(r^{-d}), r \to \infty$, where d is the dimensionality of the problem.

match the mean total kinetic energy to kinetic energy of thermal motion

$$E_{th} = N_{deg}\frac{kT}{2}, \tag{1.11}$$

where N_{deg} is the number of degrees of freedom, k Boltzmann constant and T temperature. The coupling method is equipped with stochastic algorithms in order to ensure the ergodicity of the system.

Classical MD emerged as a powerful and versatile tool in computational biochemistry as it provided insight into dynamics as well as statistical description of large molecular systems such as proteins or nucleic acids, where quantum effects can be neglected. Therefore most of the methodology is optimised for the biochemical and biophysical purpose. Nevertheless, the increase in computational efficiency and general appreciation of the MD methods trod the path for applications in a variety of complex molecular systems, to which Langmuir monolayers belong.

The overall structural properties of various surfactant monolayers were studied previously; for instance, McMullen and Kelty [11] focused on the effect of methyl group in 18-methyleicosanoic acid on molecule packing properties in contrast to eicosanoic (arachidic) acid, whereas Chanda and Bandyopadhyay [12] studied structural parametres of $C_{12}E_6$, one of the most common noionic surfactants in industrial use.

The effect of the monolayers on water transmission across the interface has been studied as well. Concerning inverse micelles in marine aerosol environment, Takahama and Russell [13] examined water uptake on atmospherically relevant surfaces, having performed simulations of octanoic and myristic acid monolayers; Henry *et al.* [14] studied octadecanol on water to investigate the ability of the Langmuir monolayer to reduce water evaporation.

Attempts to calculate the pressure-area isotherm of a Langmuir monolayer from the MD simulations have been reported recently; Baoukina and coworkers [15] employed a coarse-grained forcefield to obtain the surface pressure in dipalmitoyl-phosphatidylcholine monolayer.

The results of an MD simulation may vary depending on the forcefield used, thus benchmarking of common forcefields is an important issue. Only recently, Plazzer and coworkers [16] published a study comparing performance of OPLS/AA, COMPASS and GROMOS96 ff53a6 forcefields in simulations of Langmuir monolayer of octadecanol. Performance studies of commonly used classical MD forcefields for fatty acid monolayers have not been reported.

2. Technical Background

2.1 Palmitic acid systems

The simulations of a Langmuir monolayer of palmitic acid ($CH_3(CH_2)_{14}COOH$,PA), which are the subject of the analysis in the present thesis, mimic a typical compression experiment in a Langmuir trough [2]. The simulation box contains two monomolecular layers of PA separated by a water slab; a vacuum layer is placed above and below the PA monolayers. The box was gradually compressed along the lateral (i. e. parallel to the water surface) dimensions and for selected box sizes a production MD run was subsequently carried out. The simulation details are given below.

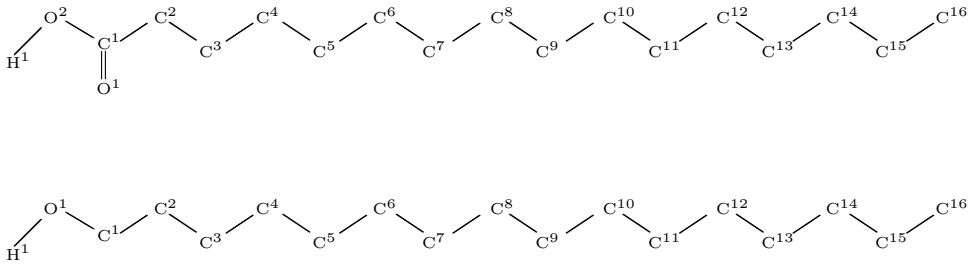

Figure 2.1: A sketch of palmitic acid (top) and 1-hexadecanol (bottom) chains with their headgroups.

2.1.1 Small systems

The original MD simulations were performed by K. Kovalčíková at the International Summer School 2010 in Nové Hrady [17]. The system consisted of a total of 58 palmitic acid molecules arranged in two monolayers separated by a water slab of 863 molecules. The box size was varied from 2.1 to 3.0 nm in the x and y dimension so as to achieve surface densities represented by area per molecule in the range from 0.15 to 0.31 nm^2. The box size in the z dimension (perpendicular to the water surface) was kept at 12 nm in order to restrain the monolayer periodic replicas from interacting with each other in this direction, creating a vacuum spacing above both monolayers. The simulations were run for 2 ns.

2.1.2 Large systems

Due to symptoms of insufficient equilibration in the small systems a new set of NVT simulations was carried out by M. Khabiri in the group of Dr. M. Roeselová at IOCB. Two simulations were performed by the author of the thesis with kind advice of M. Khabiri. The simulation length was extended to 20 ns and the box size was doubled in the x and y dimension. Therefore, the large systems consisted of 232 palmitic acid and 6770 water molecules total. Table 2.1 lists

the box dimensions for each simulation in the large set, as well as corresponding surface area per PA molecule, which is used as a reference in the analysis. The structural parametres of the monolayer were averaged over final 10 ns of the simulation trajectory.

x	y	z	area/molec.
	[nm]		[nm^2]
4.7	4.7	30	0.19
4.8	4.8	25	0.20
5.0	5.0	30	0.22
5.2	5.2	30	0.23
5.4	5.4	15	0.25
5.6	5.6	15	0.27
5.8	5.8	15	0.29
6.0	6.0	15	0.31
6.2	6.2	15	0.33
6.4	6.4	15	0.35
6.6	6.6	15	0.38

Table 2.1: Simulation box dimensions.

2.2 Hexadecanol system

We ran simulations of 1-hexadecanol ($CH_3(CH_2)_{15}OH$) monolayer at various surface densities to compare chain length and dihedral angle distributions with the results for palmitic acid. The systems consisted of 64 alcohol molecules in each of the two monolayers, separated by a water slab of 1192 molecules. The simulation box, starting at 3.4×3.4×8.8 nm^3 (mean area per molecule 0.18 nm^2) was gradually extended by 0.2 nm in x and y direction and 2 ns MD production run was carried out for each box size until 4.4×4.4×8.8 nm^3 (mean area per molecule 0.30 nm^2) reached. For the purpose of comparison to palmitic acid, we analysed the last nanosecond of each of the three trajectories from the resulting set of simulations at mean molecular areas of 0.20, 0.25 and 0.30 nm^2.

2.3 Forcefield parametres

The geometry of the palmitic acid molecule was optimised by an *ab inito* calculation, employing MP2 method with the *6-31G** basis set. The HF method with *6-31G** basis set, followed by RESP routine, was used to obtain the partial charges at the atom sites. The MP2 method with *aug-cc-pvDZ* basis set was used to determine the partial charges and to optimise the geometry of the hexadecanol molecule. The calculations were performed by Gaussian 09 [18] software suite.

The classical MD simulations of both palmitic acid and hexadecanol employed all-atom OPLS[1] forcefield [4] to model the monolayer, while SPC/E [19] was used for water.

[1]Optimised Potentials for Liquid Alcohols

2.4 Simulation details

Apart from the system composition, simulation box size and simulation length, the remaining parametres were identical for all simulations discussed above. The leap-frog algorithm (1.9)-(1.10) with 2 fs time step was used to integrate the equations of motion. The atom coordinates were saved every thousand steps, i. e. every 2 ps. Bond lengths were constrained using LINCS (LINear Constraint Solver) algorithm [20]. Electrostatic forces were evaluated using PME [8] and 1.0 nm cutoff distance was used for both Lennard-Jones potential and the short-range part of Ewald sum. Temperature was maintained at 310 K using velocity rescaling [10].

2.5 Programs and utilities

2.5.1 GROMACS

GROMACS 4.0.7 [21] software package was used to carry out the simulations and for the subsequent analysis. The abbreviation GROMACS stands for *GROningen MAchine for Computer Simulations.* It is a system for performing MD simulations and energy minimisation. GROMACS was originally developed in University of Groningen in Netherlands, however universities in Uppsalla and Stockholm share core develompent and contribution maintenance at present. It is free software, licensed under GNU/GPL (GNU General Public Licence) [22]. GROMACS supports all forcefields used to date [7], is customisable and comes with a set of analysis tools. For our purpose, the analysis utilities `g_angle`, `g_density` and `g_sgangle` were used.

Gromacs file structure

The essentials for starting a simulation are the initial coordinates of the system (GROMACS coordinate files have extension `*.gro`, though `*.pdb` is generally supported), topology file with forcefield parametres (`*.top`, `*.itp`) and a setup file (`*.mdp`) configuring the simulation options, all in human-readable ASCII format. The data from these three files are gathered by GROMACS preprocessor `grompp` and saved in a run-input file (`*.tpr`), containing all the information for the integrator. Unlike the original files, `*.tpr` is a binary file. The simulation is carried out by `mdrun`. Positions, velocities, and forces are stored in a trajectory file with extension `*.trr` or `*.trj`; a compressed trajectory file containing only atom positions is in `*.xtc`. The precision of the coordinates can be optionally downgraded.

2.5.2 Visualisation and Graphics

One of the most popular tools to visualise MD trajectories is VMD (Visual Molecular Dynamics) developed at University of Illinois [23]. We used VMD version 1.8.7 to prepare the system snapshots. For plotting the figures we utilised *gnuplot* and final processing of graphics was done by GIMP (GNU Image Manipulation Program.) Details on these programs can be found in [24, 25].

3. Results and Discussion

The main objective of this thesis is to analyse the aforementioned simulations of palmitic acid monolayer. For each box size the following structural parametres were computed:

- Tilt angle of the acid chains
- Chain length
- Dihedral angles
- Number density profiles
- Monolayer thickness

3.1 Palmitic acid

The **snapshots** of the final[1] configuration were obtained using VMD and are given in the attached Graphics Supplement. The figure sums up the general behaviour of the monolayer with respect to surface densities considered; when the area per molecule is low, the molecules pack tightly and are in nearly vertical position. Some of them are forced to immerse deeper in the water or are lifted above other molecules' headgroups, thus the water-monolayer interface is rippled, which is typical for compression near the collapse limit. The maximal surface density examined in the large systems – 0.19 nm^2 per molecule – is not, however, large enough to exhibit complete exclusion of the PA chains from the monolayer. At 0.20 nm^2 per molecule, the chains start to tilt and with increasing area per molecule the monolayer-water interface flattens and the palmitic acid chains are more tilted, as they have more space. At the same time, the thickness of the monolayer decreases. At 0.35 nm^2/molecule, the monolayer homogeneity is broken and the pores appear.

The **tilt angle** α of PA chains was computed as the angle between the vector connecting the C^1 and C^{16} atoms and the z axis, representing the normal to the water surface. First, we calculated the tilt angle distributions for small systems; the distributions for three selected surface densities are given in Figure 3.1. The tilt angle distributions differ from the expected ones; each distribution in Figure 3.1 exhibits a secondary peak, indicating of a population of alkyl chains, whose tilt angle is significantly larger than in the main population. A region of such tilted alkyl chains was found close to the border of the simulation box in visualisation of the trajectories. We therefore found the systems insufficiently equilibrated. This led to preparation of the larger systems with longer simulation time as mentioned in the Section 2.1.2. The following results, as well as the snapshots in the Graphics Supplement, concern the large systems only, unless stated otherwise.

The tilt angle distributions for four selected surface densities of the large systems are plotted in Figure 3.2. We observe that with increasing area per molecule the tilt angle increases, as can be seen from the Graphics Supplement

[1] i. e. at the end of the 20 ns trajectory.

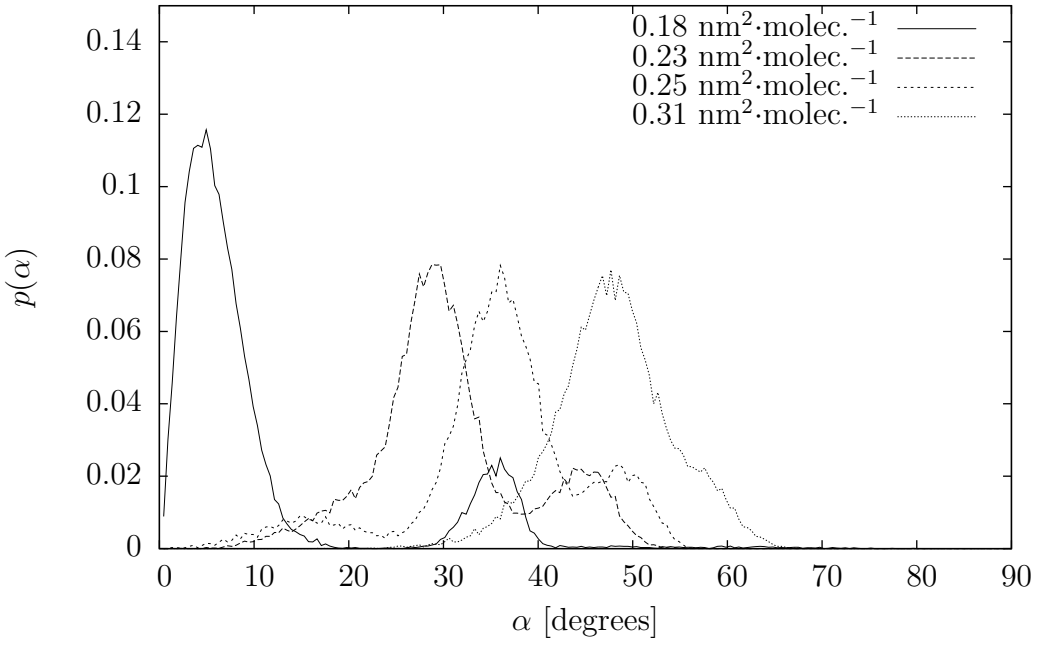

Figure 3.1: Tilt angle distributions for selected surface coverages in the small palmitic acid system.

as well. The average tilt angles with respect to surface density of the monolayer (represented by the area per molecule for all box sizes analysed) are plotted in Figure 3.3 in comparison to experimental data by Weidemann *et al.* [3]. The tilt angle in [3] was originally measured as a function of surface pressure; to enable comparison, we used the pressure-area isotherm measurements by Sierra-Hernández and Allen (Figure 1.2,[2]) and thereby obtained the corresponding area per molecule, against which the tilt angle in Figure 3.3 is plotted. The agreement of the simulation data with the experiment is fairly good. Though the data from experiment [3] do not fall within our errorbars of standard deviations [26], the angles we obtained show similar trend, being close to the experimental values. The difference between the experimental and calculated values can be ascribed to different temperature in the experiment, as Weidemann and coworkers performed their measurements at 24°C (the pressure-area isotherm [2] was obtained at 22°C,) while the thermostat in the MD simulations was set at 310 K, i. e. 37°C. The monolayer is assumed to be more organised at lower temperatures; hence the experimental tilt angle value is lower in comparison to the simulations. A sudden change in the trend is observed at 0.35 nm^2 per molecule; this is due to occurence of pores in the monolayer structure, as can be seen from the Graphics Supplement. The change of slope at 0.22 nm^2 per molecule, suggesting of 2D-liquid to 2D-crystal phase transition [14], is notable as well.

Our data agree well with the results for octadecanol by Plazzer and coworkers [16], particularly concerning their systems modeled by OPLS. Their variances are rather smaller, which we assume is due to enhanced internal correlation between the alkyl chains caused by smaller system size used in their case.

The **chain length** l was computed as the distance between C^1 and C^{16} atoms of the palmitic acid chain. A distribution of the lengths for three surface densi-

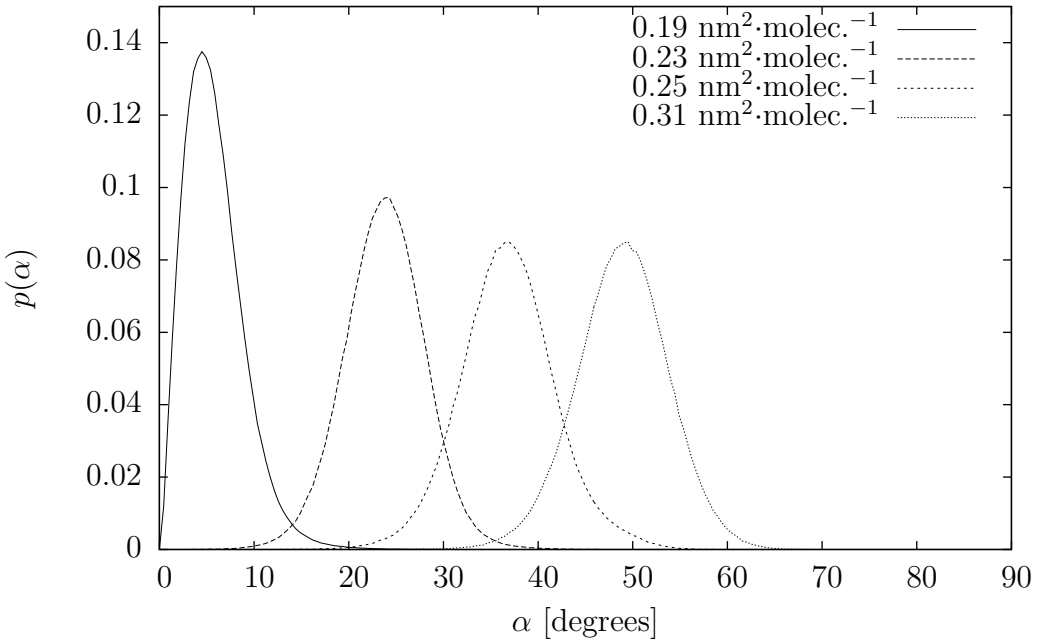

Figure 3.2: Chain tilt angle distributions for selected surface densities in the large palmitic acid system.

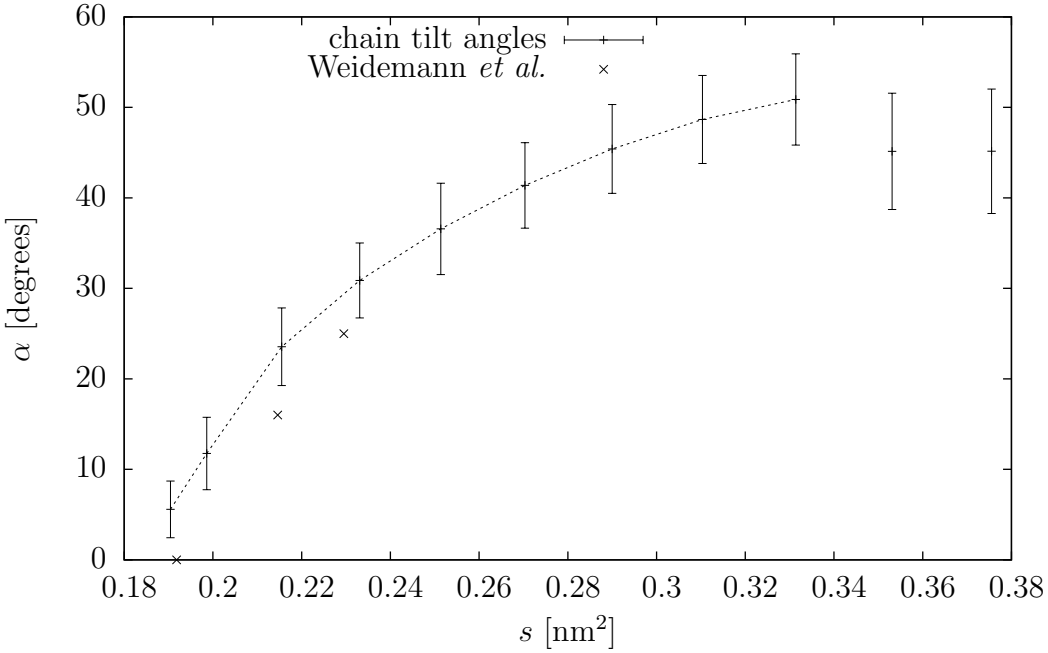

Figure 3.3: Average chain tilt angles of palmitic acid monolayer.

ties can be found in Figure 3.4. The distribution was found to be bimodal for all surface densities. Corresponding peak positions along with FWHM[2]s are in Figure 3.5.

The maxima of the distributions are located in the vicinity of 1.84 and 1.91 nm, respectively. Considering 0.154 nm for C-C bond length and 109.47° for C-C-C bond angle, simple calculations yield the all-*trans* PA chain length value of 1.888 nm. In the case of a gauche defect in the C^1-C^2-C^3-C^4 or C^{13}-C^{14}-C^{15}-C^{16} dihedral the chain length assumes a value of 1.810 nm. The slightly higher positions of both peaks in the distributions can be rationalised in terms of changes in chain geometry due to the intermolecular interactions and the thermal motion at ambient temperature.

Our expectation of the chain length behaviour, based on the published results for octadecanol [14], was that the palmitic acid chains are all fully extended at low area per molecule, so that the corresponding distribution would show one narrow peak. As the area per molecule increases, the fraction of shorter chains due to gauche defects is supposed to increase; we expected the distributions to become broader, with the height of the main peak decreasing.

Instead, the PA chain length distributions we obtained from the simulations exhibit more complicated behaviour. In addition to the bimodality of the distributions, there is no clear trend with respect to the area per molecule[3] as far as the height of the two peaks in the distribution is concerned.

To search for the source of bimodality in the palmitic acid chain length distribution, we also decided to investigate **dihedral angle** distributions. Since it is reasonable to expect that the central part of the alkyl chains remains fully extended due to tight packing of the molecules, the distributions were computed for selected bonds in the vicinity of chain ends. In the following discussion, the dihedral angle of 180° represents *trans* conformation, while angle value lower than 120° or higher than 240° corresponds to the *gauche* conformation. Figure 3.6 shows the O^2-C^1-C^2-C^3 dihedral angle distribution, which can be also viewed as the measure of rotational freedom of the headgroup. However, this dihedral angle value does not affect the chain length. The distribution peaks at 180° and two minor peaks are visible at approximately 70° and 290°. The fraction of dihedrals in *gauche* conformation is not as high as for octadecanol [16, 14] as a consequence of different headgroup structure.

The dihedral angle distribution for the neighbouring atom group, C^1-C^2-C^3-C^4, is in Figure 3.7. A considerable fraction of the chains, varying from one half to two thirds, was observed to have the *gauche* conformation. Moreover, the fraction of the *trans* and *gauche* conformations appears correlated to chain length populations of 1.91 and 1.84 nm, respectively. At 0.19 and 0.31 nm^2 per molecule the *trans* fraction is substantially higher than at 0.23 and 0.25 nm^2 per molecule. The PA chains are tightly packed at 0.19 nm^2 per molecule; the packing

[2]Full width at half maximum.

[3]From the analysis of the small systems it turned out that the high ordering characterised by all-*trans* conformation prevalence appears at surface densities around 0.16 nm^2 per molecule, which were not included in the large systems set, as exclusion of PA chains from the monolayer occured at this surface density. We observed the distributions to be almost identical for both small and large systems at corresponding surface densities regardless the insufficient equilibration of the small systems. The tilt angle distribution therefore seems to provide better measure of the monolayer equilibration compared to the chain length distribution.

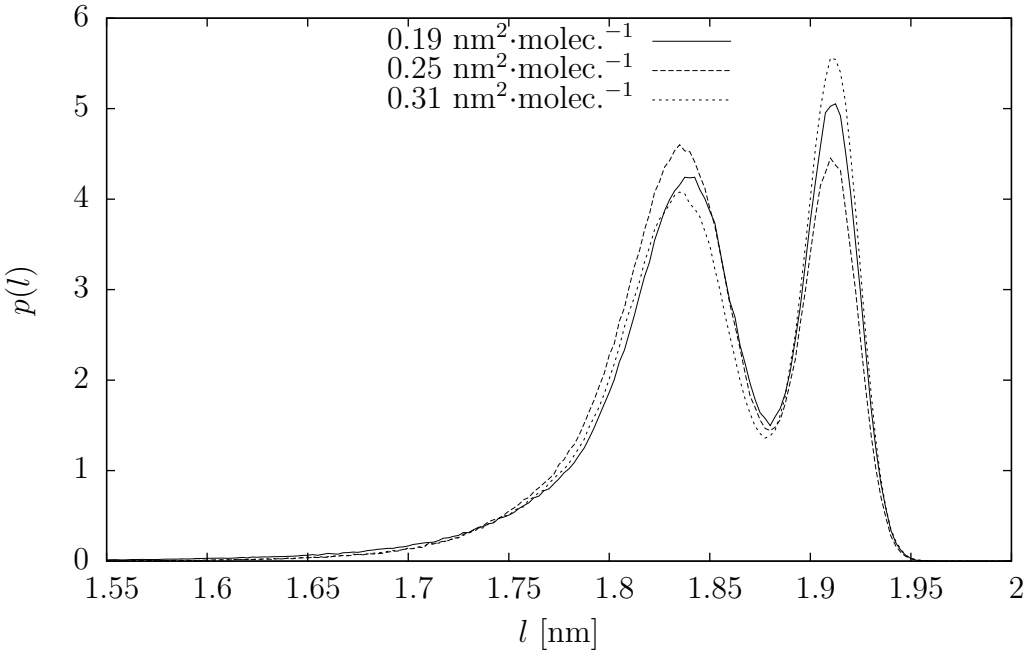

Figure 3.4: PA chain length distributions for selected surface densities.

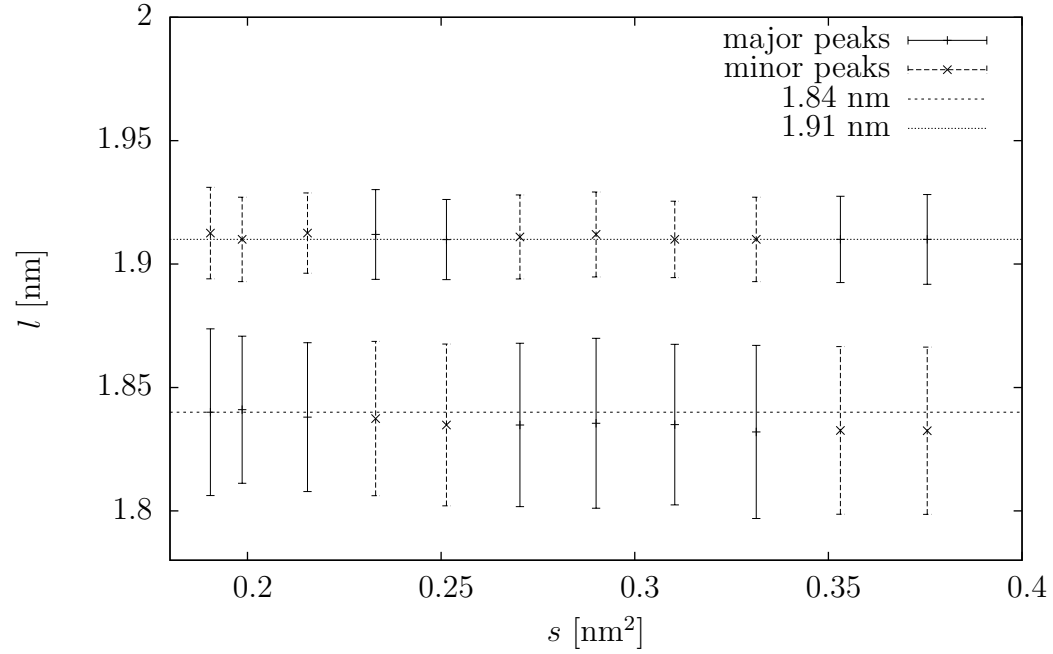

Figure 3.5: PA chain length peak positions.

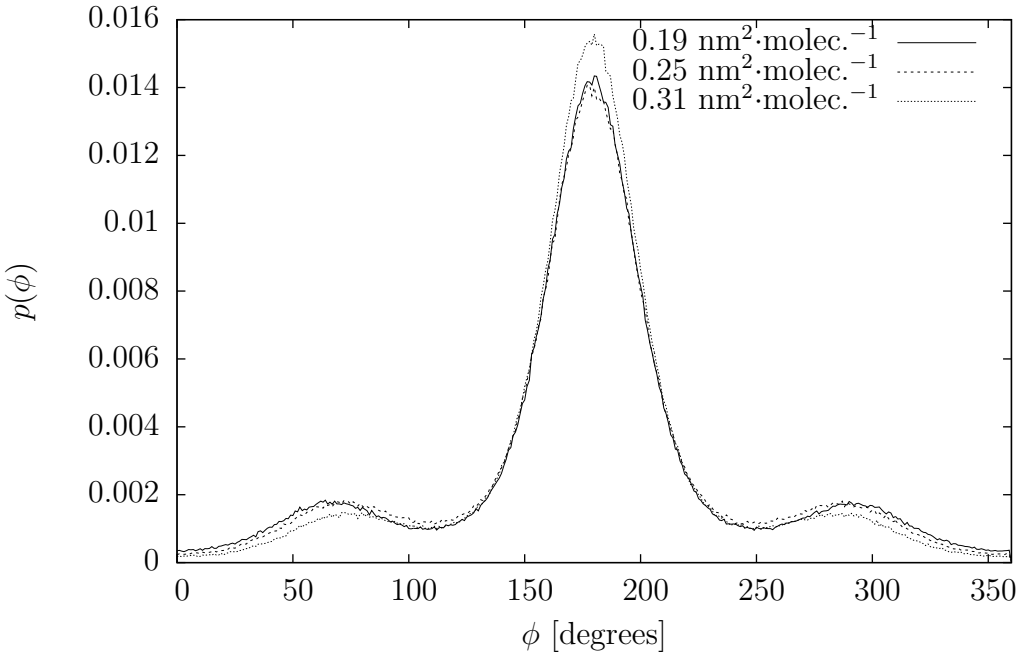

Figure 3.6: O^2-C^1-C^2-C^3 dihedral angle distribution.

results in straightening of the chains. However, at the surface density of 0.31 nm^2 per molecule, being close to the point of the pore occurence, the monolayer is stretched, so the alkyl chains are forced to straighten up again. This behaviour is seen in the corresponding length distribution as well. The assumption of strong correlation between this dihedral and the chain length in palmitic acid monolayer therefore seems plausible.

The C^1-C^2-C^3-C^4 dihedral angle distribution is also correlated with deeper immersion of PA chains in the water. The trajectory visualisations indicate that the chain bends when the headgroup is immersed deeper into water, probably due to headgroup-headgroup interactions. The bend is viewed as the change in this dihedral angle; Figure 3.8 elucidates the chain conformations.

The C^{13}-C^{14}-C^{15}-C^{16} dihedral angle distribution is shown in Figure 3.9. The *trans* conformation prevails. For remaining dihedral angles we examined (C^{12}-C^{13}-C^{14}-C^{15}, C^{11}-C^{12}-C^{13}-C^{14}, C^{10}-C^{11}-C^{12}-C^{13},C^9-C^{10}-C^{11}-C^{12}) the distributions are almost identical, slight differences occur with increasing box size as the torsional freedom of the chains increases. These results are in qualitative agreement with conclusions of McMullen and Kelty [11], who found that the tail region of the fatty acid chains is more ordered than the headgroup.

The **number density profiles** ρ_n were computed with 0.1 nm resolution along the z axis and **monolayer thickness** t was extracted from them as FWHM of the averaged density profile of the monolayer. The average was taken from monolayers at both interfaces. The density profiles are plotted in Figure 3.10. As expected for incompressible liquid, water density in the bulk region remains constant for all lateral (x and y) box dimensions of the system, approximately 100 molecules per nm^3, a standard value for SPC/E water [14]. Thus, when the lateral dimensions of the simulation box decrease, the thickness of the water layer increases. The thickness of the PA monolayer increases with decreasing monolayer

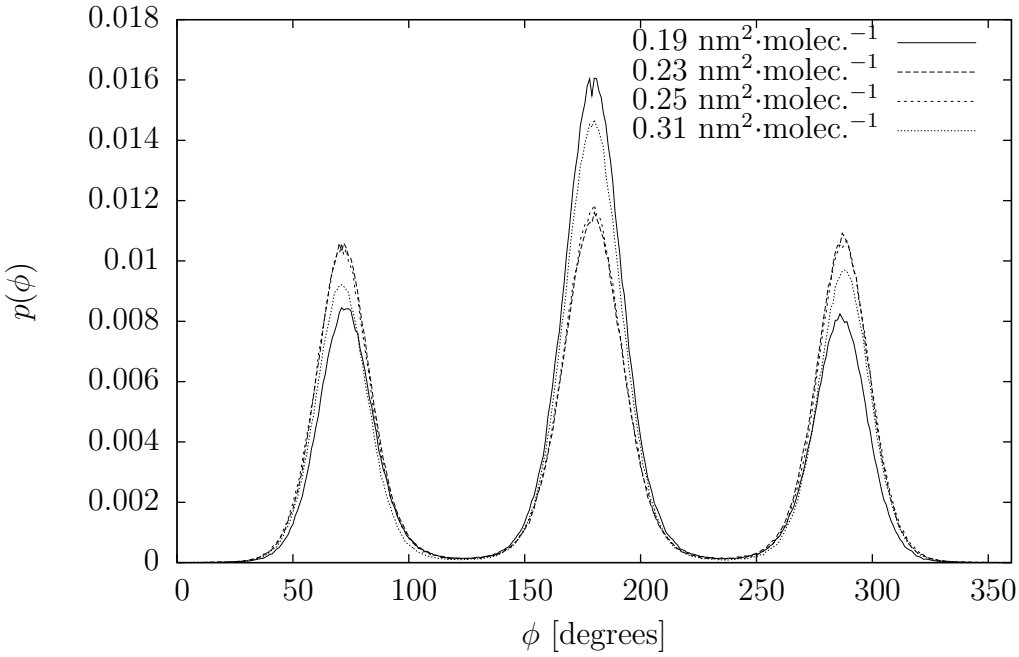

Figure 3.7: C^1-C^2-C^3-C^4 dihedral angle distribution for palmitic acid.

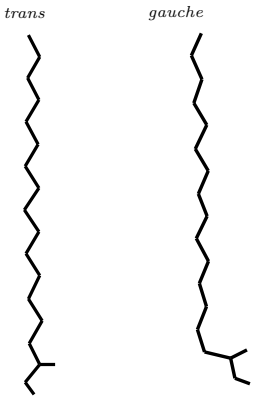

Figure 3.8: Two typical conformations of the palmitic acid chain.

area as well; as the system is more compressed, the chains are less tilted, heading towards "stand-up" position. A sudden change in the monolayer structure at 0.38 nm^2 is apparent in the density profile, as the curve is significantly lower and lacks the plateau. From the snapshots in the Graphics Supplement, it can be seen that the molecules aggregated, leaving a region of uncovered water surface – a pore. The partial penetration of water molecules through the pore is also viewed in a somewhat less steep slope of the water density profile in the interface region.

A plot of average monolayer thickness with respect to area per molecule is given in Figure 3.11. The data were fitted to a function $f(x) = \frac{c}{x}$ using *gnuplot*, as we assume that the molecules pack tightly and maintain their volume, hence the volume of the monolayer is conserved. The parametre value yielded by the fit is $c = (0.4090 \pm 0.0014)$ nm^3. As it can be seen from the corresponding figure, for all surface densities considered up to the last two the agreement with this assumption is satisfactory, showing that the palmitic acid density is indeed con-

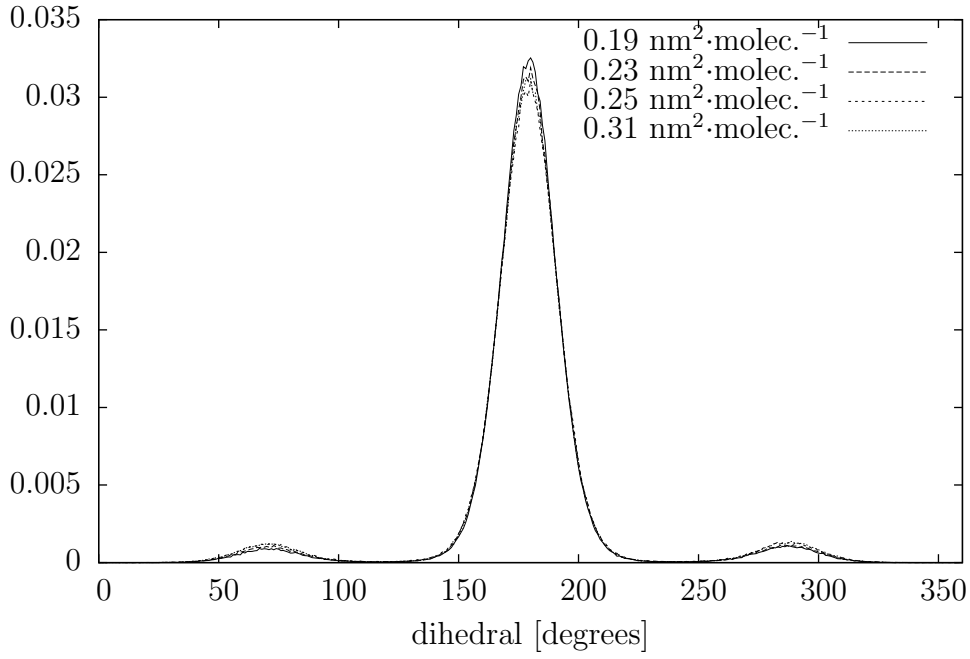

Figure 3.9: C^{13}-C^{14}-C^{15}-C^{16} dihedral angle distributions for PA.

served throughout the simulations. The disagreement for the 0.33- and 0.35- nm^2 systems is due to the fact that the monolayer is not 2-D homogeneous any more.

3.2 Comparison to hexadecanol

Since the chain length distribution of octadecanol with respect to surface density shows qualitatively different behaviour [14] to that of palmitic acid, we decided to carry out simulations of hexadecanol monolayer with the aim to directly compare the chain length and dihedral angle distribution to the results for PA, as both hexadecanol and palmitic acid molecules have the same number of carbon atoms. The chain length distribution for hexadecanol, computed identically as for palmitic acid, is given for three surface densities in Figure 3.12. The histograms do not resemble those for palmitic acid, but are rather similar to the octadecanol chain length distributions in [14]. A peak in the vicinity of the all-*trans* length of 1.91 nm is dominant, lowering and moving to the left (i. e. towards lower chain lengths) with increasing area per molecule. At the same time the "shoulder" of the histogram turns into a secondary peak, indicating that the fraction of *gauche* defects among the chains increases; the fraction of the *gauche* conformations is, however, much lower than for PA.

In the case of palmitic acid, we attributed the bimodality in the chain length distribution to the almost even contributions of the *trans* and *gauche* conformations in the C^1-C^2-C^3-C^4 dihedral angle. A comparison to the distribution of this dihedral angle in hexadecanol, as seen in Figure 3.13, confirms this conclusion. The C^1-C^2-C^3-C^4 dihedral angle distribution in hexadecanol is strongly dominated by *trans* conformation at 180°. At 0.20 nm^2 per molecule, the *gauche* conformations almost vanish; small fraction of the *gauche* conformations appears at 0.25 and 0.31 nm^2 per molecule, being higher for the lower surface density.

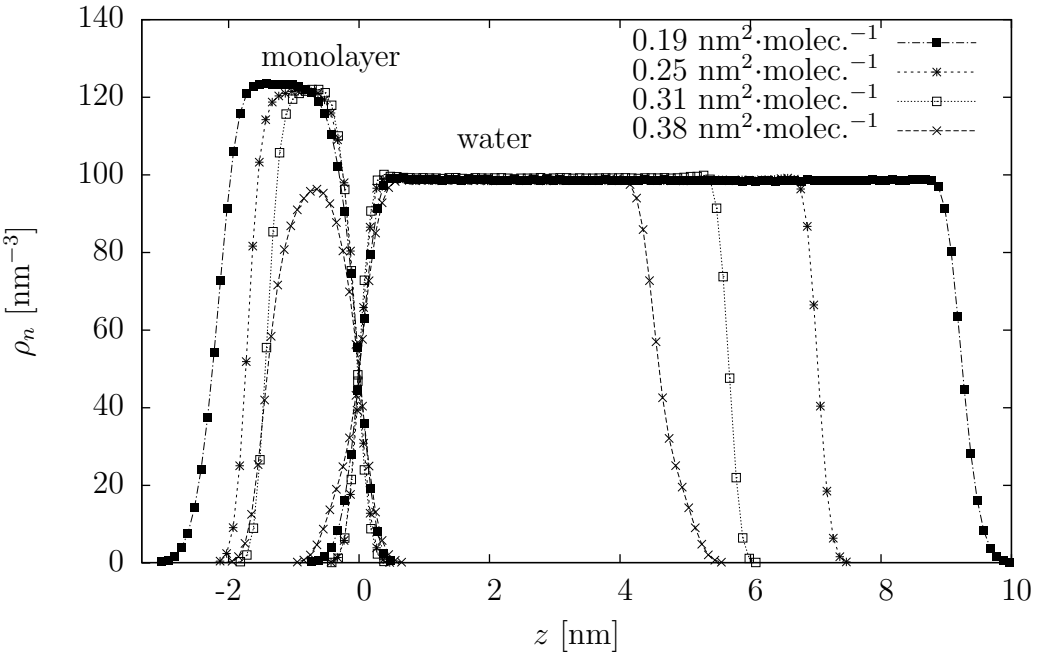

Figure 3.10: Average number density (ρ_n) profiles of the PA monolayer and water for selected surface densities.

The height of the *trans* peak at 180° increases with decreasing area per molecule.

We also measured the O^1-C^1-C^2-C^3 dihedral angles in hexadecanol chains. The corresponding distribution is given in Figure 3.14. The fraction of *gauche* conformations is higher than the results published for octadecanol [14, 16]. While both published simulations were also performed using OPLS forcefield, the authors did not supply partial charges, which are assumed to influence the molecular conformations.

In summary, the chain length and the C^1-C^2-C^3-C^4 dihedral angle distributions showed significant differences between the palmitic acid and hexadecanol monolayer behaviour. The palmitic acid headgroup interacts with water more strongly in comparison to hexadecanol due to the presence of an extra oxygen atom in the headgroup moiety. When the PA chain is is immersed deeper into water, the chain bends, which results in change in the C^1-C^2-C^3-C^4 dihedral angle, while the PA headgroup tends to maintain its torsional orientation around the C^1-C^2 axis so that the O^2-C^1-C^2-C^3 dihedral mostly remains at 180°. Conversely, the hexadecanol headgroup rotates around the C^1-C^2 axis, whereas the C^1-C^2-C^3-C^4 dihedral angle remains in the *trans* conformation. This holds regardless the quantitative difference in alcohol headgroup orientational preferences between our results and [14, 16].

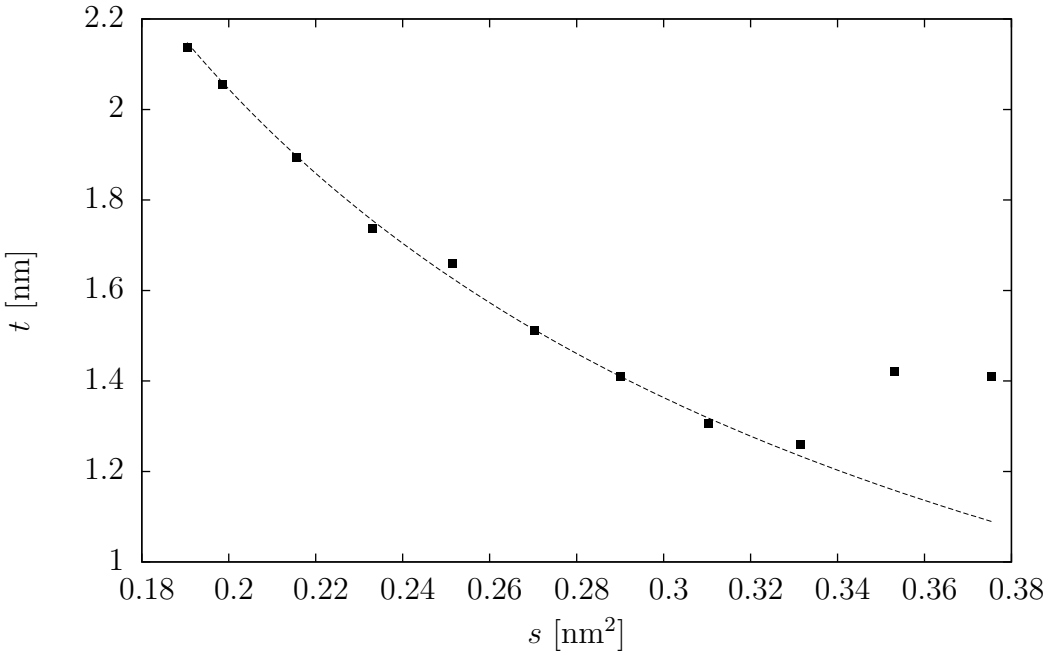

Figure 3.11: PA monolayer thickness depending on area per molecule fitted to $\frac{c}{x}$.

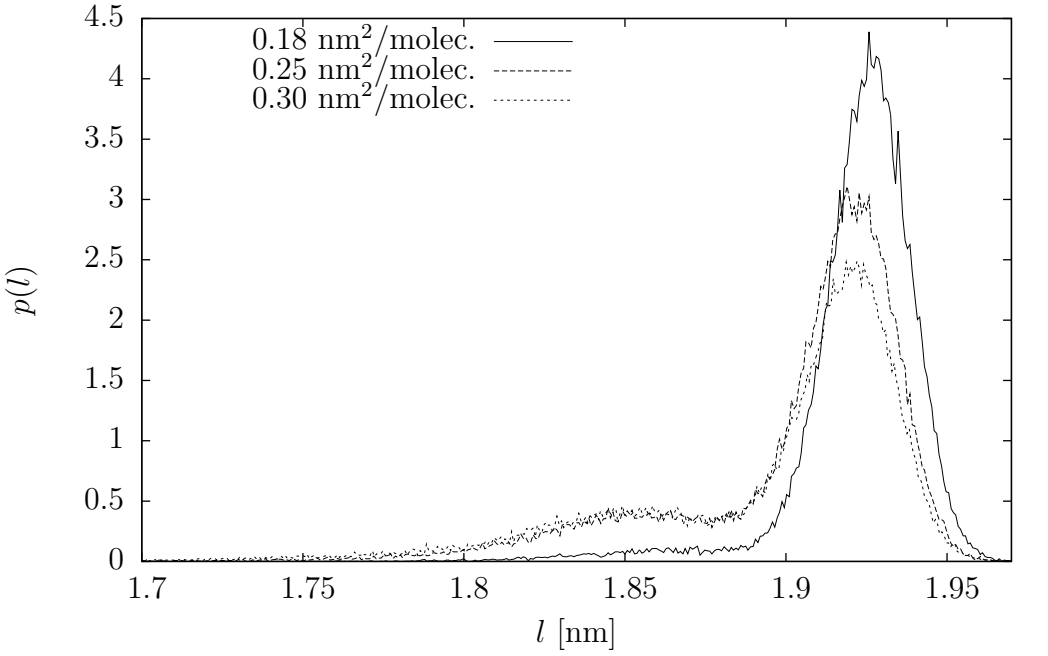

Figure 3.12: Hexadecanol chain length distribution.

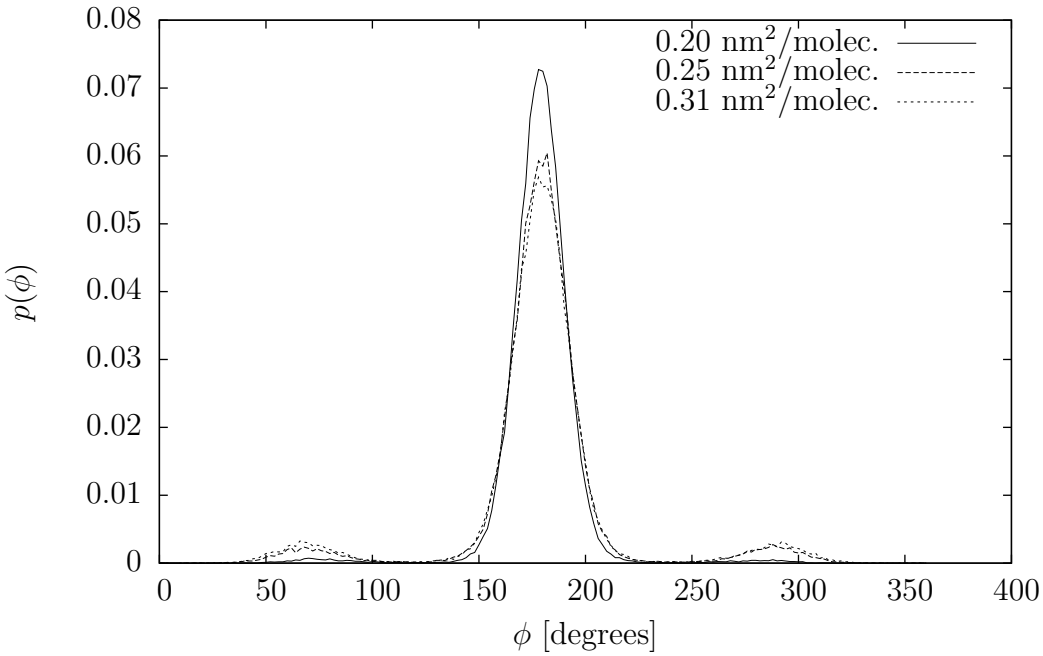

Figure 3.13: C^1-C^2-C^3-C^4 dihedral angle distribution in hexadecanol.

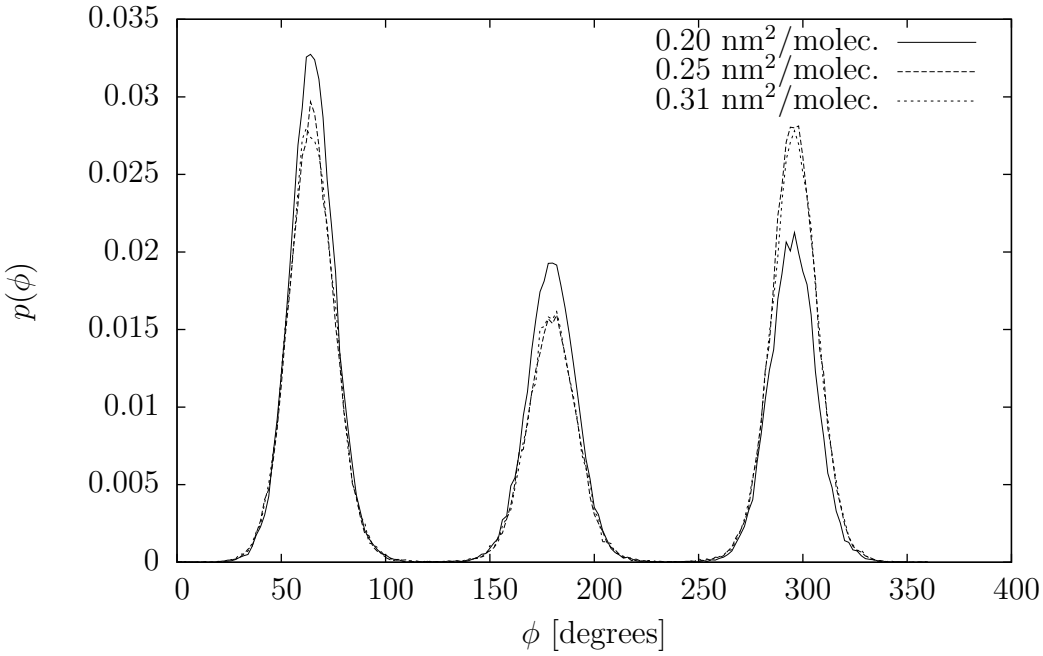

Figure 3.14: O^1-C^1-C^2-C^3 dihedral angle distribution in hexadecanol.

Conclusions

We analysed MD simulations of palmitic acid monolayer at the water-air interface for different compression stages of the monolayer.

The main results can be summarised as follows:

- The OPLS forcefield used in the simulation of palmitic acid reproduces well the overall structural behaviour of Langmuir monolayers as reported in the literature.
- We have found good agreement of the PA chains tilt angle with available experimental works. The tilt angle increases with increasing area per molecule until 0.35 nm^2, where pores in the monolayer appeared and a sudden decrease in the tilt angle was observed.
- The chain length of palmitic acid has a bimodal distribution for all surface densities examined. We attributed the phenomenon to the C^1-C^2-C^3-C^4 dihedral angle distribution, with almost equal preference of the *trans* and *gauche* conformations.
- We ran simulations of 1-hexadecanol for comparison. The chain length distribution for hexadecanol was found consistent with the octadecanol MD simulations published in the literature, showing qualitatively different behaviour from that of palmitic acid.

Perspectives

Fatty acid monolayers are believed to affect rotational and translational dynamics of the water molecules at the interface, which in consequence may influence freezing of organic-coated aerosol particles. The orientational distribution of water molecules with respect to distance from the monolayer as well as mean square displacements may be calculated to get complete structural and dynamical information about the monolayer-water interface. The orientational analysis of water molecules was originally a part of the assignment but it was not performed as it could not be done properly due to lack of time.

In addition to the results presented, we also carried out further structure analysis, such as the CH_3 endgroup orientation, which can be determined experimentally via SFG spectroscopy [2]. However, these results are somewhat dubious at the present stage and require more detailed analysis, as well as the radial distribution functions (RDF) we calculated, which show ambiguous behaviour with respect to the area per molecule. Nonetheless, the RDFs are essential in hydrogen bonding examination. The water-headgroup and headgroup-headgroup interaction should further explain the difference between alcohol and carboxylic acid headgroup properties, which are assumed to affect the alkyl chain conformational behaviour.

The ultimate benchmarking of the model to the experiment would be calculating the surface pressure in the monolayer, hence obtaing the entire pressure-area isotherm from the simulations. This goes far beyond the scope of present study, particularly due to long simulation time required. The calculations are currently underway in the group of Dr. M. Roeselová at IOCB.

Bibliography

[1] Ulman, A.: *An Introduction to Ultrathin Organic Films.* Academic Press, London, 1991.

[2] Sierra-Hernández, R. M.; Allen, H. C.: *Incorporation and Exclusion of Long Chain Alkyl Halides in Fatty Acid Monolayers at the Air-Water Interface.* Langmuir, **2010**, 26(24), 18806-18816.

[3] Weidemann, G.; Brezesinski, G.; Vollhardt, D.; Bringezu, F.; de Meijere, K.; Mohwald, H.: *Comparing Molecular Packing and Textures of Langmuir Monolayers of Fatty Acids and Their Methyl and Ethyl Esters.* J. Phys. Chem. B, **1998**, 102, 148–153.

[4] Jorgensen, W. L.: *Optimized Intermolecular Potential Functions for Liquid Alcohols.* J. Phys. Chem., **1986**, 90, 1276-1284.

[5] Rapaport, D. C.: *The Art of Molecular Dynamics Simulation.* Cambridge University Press, Cambridge, 1995.

[6] *Numerical Recipes Numerical Recipes in Fortran 77: The Art of Scientific Computing.* University Press, Cambridge, 1992.

[7] van der Spoel, D.; Lindahl, E.; Hess, B; van Buuren, A. R.; Apol, E; Meulenhoff, P. J.; Tieleman, D. P.; Sijbers, A. L. T. M.; Feenstra, K. A.; van Drunen, R.; Berendsen, H. J. C: *Gromacs User Manual version 4.5* (2010). `http://www.gromacs.org`

[8] Darden, T.; York, D.; Pedersen, L.: *Particle mesh Ewald: An* $N \cdot \log(N)$ *method for Ewald sums in large systems.* J. Chem. Phys., **1993**, 98, 10089-10093.

[9] Callen, H. C.: *Thermodynamics and Introduction to Thermostatistics.* 2^{nd} ed., John Wiley & Sons, New York, 1985.

[10] Bussi, G.; Donadio, D.; Parinnelo, M.: *Canonical sampling through velocity rescaling.* J. Chem. Phys., **2007**, 126, 014101.

[11] Kelty, S.P.; McMullen R.L.: *Molecular Dynamics Simulations of Eicosanoic Acid and 18-Methyleicosanoic Acid Langmuir Monolayers.* J. Phys. Chem. B (Letters), **2007**, 111, 10849-10852.

[12] Chanda, J; Bandyopadhyay, S: *Molecular Dynamics Study of a Surfactant Monolayer Adsorbed at the Air/Water Interface.* J. Chem. Theory Comput., **2005**, 1, 963-971.

[13] Takahama, S.; Russell L. M.: *A molecular dynamics study of water mass accommodation on condensed phase water coated by fatty acid monolayers.* J. Geophys. Res., **2011**, 116, D02203.

[14] Henry, D.J.; Dewan, V. I.; Prime, E. L; Qiao, G.C.; Solomon, D.H.; Yarovsky, I.: *Monolayer Structure and Evaporation Resistance: A Molecular Dynamics Study of Octadecanol on Water.* J. Phys. Chem. B, **2010**, 114, 3869-3878.

[15] Baoukina, S.; Monticelli, L.; Marrink, S. J.; Tielemann, D. P.: *Pressure-Area Isotherm of a Lipid Monolayer from Molecular Dynamics Simulations.* Langmuir, **2007**, 23, 12617-12623.

[16] Plazzer, M. B.; Henry, D. J.; Yiapanis, G.; Yarovsky, I.: *Comparative Study of Commonly Used Molecular Dynamics Force Fields for Modeling Organic Monolayers on Water.* J. Phys. Chem. B, **2011**, 115, 3964–3971.

[17] *Molecular Dynamics Simulations of mixed fatty acid/alkyl halide films at the air/water interface.* Author: Kristína Kovalčíková, Supervisor Dr. Martina Roeselová. Project #21 of *Summer School Nové Hrady 2010.* `http://www.greentech.cz/scholaludus/history/schl2010.php`

[18] *Gaussian 09, Revision A.1*, Frisch, M. J.; Trucks, G. W.; Schlegel, H. B.; Scuseria, G. E.; Robb, M. A.; Cheeseman, J. R.; Scalmani, G.; Barone, V.; Mennucci, B.; Petersson, G. A.; Nakatsuji, H.; Caricato, M.; Li, X.; Hratchian, H. P.; Izmaylov, A. F.; Bloino, J.; Zheng, G.; Sonnenberg, J. L.; Hada, M.; Ehara, M.; Toyota, K.; Fukuda, R.; Hasegawa, J.; Ishida, M.; Nakajima, T.; Honda, Y.; Kitao, O.; Nakai, H.; Vreven, T.; Montgomery, Jr., J. A.; Peralta, J. E.; Ogliaro, F.; Bearpark, M.; Heyd, J. J.; Brothers, E.; Kudin, K. N.; Staroverov, V. N.; Kobayashi, R.; Normand, J.; Raghavachari, K.; Rendell, A.; Burant, J. C.; Iyengar, S. S.; Tomasi, J.; Cossi, M.; Rega, N.; Millam, N. J.; Klene, M.; Knox, J. E.; Cross, J. B.; Bakken, V.; Adamo, C.; Jaramillo, J.; Gomperts, R.; Stratmann, R. E.; Yazyev, O.; Austin, A. J.; Cammi, R.; Pomelli, C.; Ochterski, J. W.; Martin, R. L.; Morokuma, K.; Zakrzewski, V. G.; Voth, G. A.; Salvador, P.; Dannenberg, J. J.; Dapprich, S.; Daniels, A. D.; Farkas, Ö.; Foresman, J. B.; Ortiz, J. V.; Cioslowski, J.; Fox, D. J. Gaussian, Inc., Wallingford CT, 2009. `www.gaussian.com`

[19] Berendsen, H. J. C.; Grigera, J. R.; Straatsma, T. P.: *The Missing Term in Effective Pair Potentials.* J. Phys. Chem., **1987**, 91, 6269-6271.

[20] Hess, B.; Bekker, H.; Berendsen, H. J. C.; Fraaije, J. G. E. M.; *LINCS: A linear constraint solver for molecular simulations.* J. Comp. Chem., **1997**, 18, 1463–1472.

[21] Hess, B.; Kutzner, C.; van der Spoel, D.; Lindahl, E.; *GROMACS 4: Algorithms for Highly Efficient, Load-Balanced, and Scalable Molecular Simulation.* J. Chem. Theory Comp., 435, **2008**.

[22] GNU GPL ver. 3.0 (2011). `http://www.gnu.org/copyleft/gpl.html`

[23] Humphrey, W., Dalke, A. and Schulten, K., *VMD - Visual Molecular Dynamics*, J. Molec. Graphics, **1996**, 14.1, 33-38. `http://www.ks.uiuc.edu/Research/vmd/` (2011)

[24] *gnuplot* version 4.4 patchlevel 0.
`http://www.gnuplot.info/` (2011)

[25] *GNU Image Manipulation Program* version 2.6.10.
`http://gimp.sourceforge.net/` (2011)

[26] Brož, J.: *Základy fyzikálních meření*. Státní nakladatelství technické literatury, Praha, 1968.

List of Abbreviations

AMBER	Assisted Model Building with Energy Refinement – – a molecular dynamics simulation forcefield and software suite.
ASCII	American Standard Code for Information Interchange
CPU	Central Processing Unit
FWHM	Full Width at Half Maximum
GID	Grazing Incidence Diffraction, X-ray diffraction method with high surface resolution
GIMP	GNU Image Manipulation Program
GNU/GPL	GNU General Public License
GROMACS	GROningen MAchine for Computer Simulations
HF	Hartree-Fock method
IOCB	Institute of Organic Chemistry and Biochemistry of the Czech Academy of Sciences.
LINCS	LINear Constraint Solver
LJ	Lennard-Jones, type of intermolecular interaction
MARTINI	MARrink Toolkit INItiative – a coarse-grained forcefield developed by S. J. Marrink.
MD	Molecular Dynamics
MP2	Møller-Plesset method of 2^{nd} order
OPLS	Optimized Potentials for Liquid alcoholS, a forcefield for organic compounds
OPLS/AA	all atom OPLS version
PA	Palmitic Acid
PBC	Periodic Boundary Conditions
PME	Particle Mesh Ewald, method for computing electrostatic energy
RDF	Radial Distribution Funcion, a measure of probability $g(r)$ of finding a particle in the distance r.
RESP	Restrained ElectroStatic Potential fit, a method for computing the point charges from the electron density.
SFG	Sum Frequency Generation, a surface selective spectroscopic method
SPC	Single Point Charge, a widely used water model
VMD	Visual Molecular Dynamics

List of Figures

List of Symbols

γ	surface tension
π	surface pressure
s	mean area per molecule of the monolayer
ϕ	dihedral angle
x, y, z	Cartesian coordinates
α	tilt angle of the alkyl chains
l	alkyl chain length
t	monolayer thickness